Genome-wide, integrative analysis of microRNA-mediated gene regulation in human wounds reveals cooperating microRNAs as therapeutic targets

Zhuang Liu[1,†], Letian Zhang[1,†], Maria-Alexandra Toma[1], Dongqing Li[1,2], Xiaowei Bian[1], Irena Pastar[3], Marjana Tomic-Canic[3], Pehr Sommar[4]* and Ning Xu Landén[1,5]*

[1]Dermatology and Venereology Division, Department of Medicine Solna, Center for Molecular Medicine, Karolinska Institutet, 17176 Stockholm, Sweden

[2]Institute of Dermatology, Chinese Academy of Medical Sciences and Peking Union Medical College, Nanjing, Jiangsu, China

[3]Wound Healing and Regenerative Medicine Research Program, Dr Phillip Frost Department of Dermatology and Cutaneous Surgery, University of Miami Miller School of Medicine, Miami, FL, USA.

[4]Department of Plastic and Reconstructive Surgery, Karolinska University Hospital, Stockholm, Sweden

[5]Ming Wai Lau Centre for Reparative Medicine, Stockholm Node, Karolinska Institute, 17177 Stockholm, Sweden

[†]Equal contribution

*Co-senior authors

To whom correspondence should be addressed: Email: ning.xu@ki.se or pehr.sommar@regionstockholm.se

ABSTRACT

MicroRNAs (miR), as important epigenetic control factors, reportedly regulate wound repair. However, our insufficient knowledge of clinically relevant miRs hinders their potential therapeutic use. For this, we performed miR and mRNA paired expression profiling in human acute wounds and chronic non-healing venous ulcers (VU) and presented our findings on a browsable web portal (http://130.229.28.87/shiny/miRNA_Xulab/). Integrative miR and mRNA-omics analysis unraveled miR-mediated gene regulatory networks in each repair phase of the wound repair process. Importantly, we identified 17 pathologically relevant miRs exhibiting abnormal expression in VU and displaying their targetome enriched in the VU gene signature. Study of the targetome and functions of eight clinically relevant miRs in skin cells revealed that the miRs upregulated in VU (i.e., miR-34a/c-5p, miR-424-5p, miR-450-5p, miR-7704, and miR-516-5p) promoted inflammation but inhibited proliferation. In contrast, the miRs downregulated in VU (i.e., miR-218-5p and miR-96-5p) were required for cell growth and activation. Moreover, we demonstrated miR-34a, miR-424, and miR-516 cooperativity in regulating keratinocyte growth and inflammatory response. Collectively, our study suggests that VU-dysregulated miRs cooperatively contribute to stalled wound healing characterized by failed transition from inflammatory-to-proliferative phase. Targeting cooperating miRNAs provide mew opportunity for development of clinically-relevant targeted therapy to attain higher therapeutic efficacy and specificity.

INTRODUCTION

Wound healing is a fundamental biological process comprising three sequential and overlapping phases, i.e., inflammation, proliferation, and remodeling (1). This delicate repair process is often disrupted in chronic venous insufficiency patients, resulting in venous ulcers (VU) characterized by persistent inflammation and proliferative phase initiation failure (2). VU is the most common chronic non-healing wound type, comprising 45–60% of all lower extremity ulcerations (3). VU exhibits a marked impact on health-related life quality and represents a significant financial burden both to the patients and the society with an annual health care cost of overall $14.9 billion in the USA (4). A deeper understanding of the underlying molecular gene expression regulatory mechanisms during physiological and pathological wound repair is essential for the development of more effective wound treatments (5).

MicroRNAs (miR) represent a group of short (~22 nt) non-coding ribonucleic acids, incorporating into the RNA-induced silencing complex and binding to the 3' untranslated region of their target mRNAs, resulting in mRNA destabilization and translational repression (6). Given that an individual miR can target dozens to hundreds of genes, miRs have been identified as regulators of complex gene networks (6). MiR-mediated regulation is reportedly crucial in multiple fundamental biological processes including skin wound repair (7-9). Importantly, manipulating miRs critical for the disease pathogenesis could offer a prominent therapeutic effect, supported by viral infection- and cancer-targeting miR therapeutics clinical trials (10). Therefore, miR-based therapeutics for hard-to-heal wounds represent a promising approach. However, it would require a thorough understanding of miR expression and functions in the human wound tissue (7,8,11-14). While most previous wound healing-related miR studies rely on *in vitro* or animal models, only a few have approached miR profiles in human wound tissues or primary cells from patients, including tissues and fibroblasts of diabetic foot ulcers (15,16), burn wound dermis (17), and acute wounds at the inflammatory phase (18). Despite sharing several fundamental features, the human skin structure and healing processes are different from those of the commonly used animal models (e.g., rodents) (19). Moreover, *in vitro* or animal models cannot fully simulate the human disease complexity (20,21). Thereby, a rigorous and in-depth molecular characterization of human healing and non-healing wounds would be required.

In this study, we performed paired small and mRNA expression profiling in the human skin, acute wounds during the inflammatory and proliferative phases, and VU, unraveling time-resolved changes of the whole transcriptome throughout the wound healing process and the unique gene expression

signature of a common chronic wound type. The integrative miR and mRNA omics analysis provides a network view of miR-mediated gene regulation in human wounds *in vivo* and demonstrates the functional involvement of miRs in human skin wound repair at the system level. Importantly, we identified miRs highly relevant to VU pathology, based not only on their aberrant expression but also their targetome enriched in the VU-related gene expression signature. Apart from confirming the *in silico* findings, the experimental miR expression, targetome, and function validation uncovered that VU-dysregulated miRs could act cooperatively contributing to the stalled wound healing characterized by failed transition from inflammatory-to-proliferative phase, which opens up new possibility for the development of more precise and innovative wound treatment targeting pathologically-relevant cooperating miRs to achieve higher therapeutic efficacy and specificity. Moreover, we presented these comprehensive dataset and analysis on a browsable resource web portal (http://130.229.28.87/shiny/miRNA_Xulab/) to broadly aid wound healing research.

MATERIAL AND METHODS

Human wound samples

Human wound biopsies were obtained from 10 healthy donors and 12 patients with chronic venous ulcer (VU) at the Karolinska University Hospital Solna (Stockholm, Sweden). Donor demographics are presented in Supplementary Table S1. Patients with VUs, which persisted for more than four months despite conventional therapy, were enrolled in this study (Supplementary Table S2). Tissue samples were collected from the lower extremity at the nonhealing edges of the ulcers by using a four-mm biopsy punch (Figure 1A). Healthy donors above 60 years old without skin diseases, diabetes, unstable heart disease, infections, bleeding disorder, immune suppression, and any ongoing medical treatments were recruited (Supplementary Table S3). Two full-thickness excisional wounds (4 mm in diameter) were created at the lower extremity on each donor, and the excised skin was saved as intact skin control (Skin). The wound-edges were excised with a six mm-biopsy punch at day one (Wound1) and day seven (Wound7) after wounding (Figure 1A). Written informed consent was obtained from all the donors to collect and use the tissue samples. The study was approved by the Stockholm Regional Ethics Committee and conducted according to the Declaration of Helsinki's principles.

RNA extraction, library preparation, and sequencing

RNA extraction Snap frozen tissue samples were homogenized with the TissueLyser LT (Qiagen), and total RNA was isolated using the miRNeasy Mini kit (Qiagen). RNA quality and quantity were determined by using Agilent 2100 Bioanalyzer (Agilent Technologies) and Nanodrop 1000 (Thermo Fisher Scientific Inc.), respectively.

Small RNA library preparation and sequencing The small RNA sequencing libraries were constructed using 3 µg total RNA per sample and NEB Next® Multiplex Small RNA Library Prep Set for Illumina® (NEB) following the manufacturer's recommendation. Briefly, total RNA was first ligated to adaptors at the 3' end by NEB 3' SR adaptor and 5' end by T4 RNA ligase followed by reverse transcription into cDNA using M-MuLV Reverse Transcriptase. PCR amplification of cDNA was performed using SR primers for Illumina and index primers. The PCR products were purified, and DNA fragments spanning from 140 to 160bp were recovered and quantified by DNA High Sensitivity Chips on the Agilent

Bioanalyzer. The libraries were sequenced on an Illumina Hiseq 2500 platform (Illumina, Inc.) using single-end 50bp reads, and all samples were run side by side.

mRNA library preparation and sequencing The long RNA sequencing libraries were constructed with a total amount of 2 μg RNA per sample. First, the ribosomal RNA was depleted by Epicentre Ribo-zero® rRNA Removal Kit (Epicentre). Second, strand-specific total-transcriptome RNA sequencing libraries were prepared by incorporating dUTPs in the second-strand synthesis step with NEB Next® Ultra™ Directional RNA Library Prep Kit for Illumina® (NEB). Finally, the libraries were sequenced on an Illumina Hiseq 4000 platform, and 150 bp paired-end reads were generated for the following analysis.

Analysis of miRNA-sequencing data

Quality control, mapping, and quantification Quality of raw data was assessed using FastQC v0.11.8 (http://www.bioinformatics.babraham.ac.uk/projects/fastqc/). We used mapper.pl module in the miRDeep2 v0.1.3 package (22,23) to filter low-quality reads and remove sequencing adaptors and redundancies. Trimmed reads with lengths greater than 18 nucleotides were mapped to GENCODE human reference genome (hg38) by the software Bowtie v1.2.2 (24). The miRDeep2.pl module was then performed with default parameters to identify known miRNAs, which were compared to miRNAs in miRBase release 22.1 (25). Counts of reads mapped to each known mature miRNAs were acquired from the quantifier.pl module output without allowing mismatch. miRNAs with read counts less than five in more than half of twenty samples were discarded since these miRNAs are unlikely to give stable and robust results. Raw counts of 562 miRNAs were normalized for sequencing depth using TPM methods (transcript per million = mapped read count/total reads * 10e6) (26) and prepared for further analysis.

Differential expression (DE) analysis The DESeq2 workflow (27) was carried out to fit raw counts to the negative binomial (NB) generalized linear model and to calculate the statistical significance of each miRNA in each comparison. In particular, the paired model was employed when comparing samples from the same donor. *P-value*s obtained from the Wald test were corrected using Benjamini-Hochberg (BH) multiple test to estimate the false discovery rate (FDR). The differentially expressed miRNAs were defined as FDR < 0.05 and |log2(fold change)| ≥ 1.

Principle component analysis (PCA) To explore the similarity of each sample, PCA was performed by using a DESeq2 built-in function *plotPCA* on the transformed data, in which the variances and size factors were stabilized and corrected. PCA and heatmaps were plotted by using *ggplot2* (28) and *ComplexHeatmap* (29) packages in RStudio (https://rstudio.com/).

Weighted gene co-expression network analysis (WGCNA) The normalized expression of 562 miRNAs were used as input to the WGCNA R package (30). First, we calculated the strength of pairwise correlations between miRNAs using the 'biweight' mid-correlation method. The function *pickSoftThreshold* was then employed to compute the optimized soft-thresholding power based on connectivity, which led to an approximately scale-free network topology (31). Second, a signed weighted co-expression network was constructed with a power of 18 using the one-step *blockwiseModules* algorithm (Supplementary Figure S2A). Network modules were filtered according to parameters: *minModuleSize* = 10 and *mergeCutHeight* = 0.25.

The expression profile of each module was represented by the module eigengene (ME), referred to as the first principal component of all miRNAs in each module. Pearson correlations (values from -1 to 1) and the corresponding *P-value*s between MEs and traits were computed. *P-value*s were further adjusted to FDR across all the modules using the BH method. Modules significantly associated with each trait were selected by FDR < 0.05 and absolute correlation coefficients > 0.4. The module membership (also known as kME) of each miRNA was calculated by the correlations between miRNA expression and ME. MiRNAs with the highest kME values were defined as intra-modular hub miRNAs, and networks of hub miRNAs in significant modules were visualized using the Cytoscape v3.7.2 software (32).

To check the robustness of module definition, we carried out module preservation analysis and calculated the standardized Z-scores for each module by permutating 200 times using the same 20 samples as reference and test datasets. Modular preservation is strong if Z-summary > 10, weak to moderate if 2 < Z-summary < 10, no evidence of preservation if Z-summary ≤ 2 (33).

Transcription factor (TF) enrichment analysis We leveraged a curated database about TF-miRNA regulations, TransmiR v2.0 (34), to identify the TFs regulating miRNA expression in each module. Fisher's exact tests were employed to evaluate the enrichment of each TF in the significant modules, and FDRs were adjusted to the total number of TFs (Odds ratio > 1 and FDR < 0.05). Correlations of

gene expression between TFs and miRNA modules (represented by MEs) were further filtered to identify putative TF-mediated miRNA gene expression patterns (Pearson correlation: *P-value* < 0.05, coefficient > 0). The 562 miRNAs abundantly expressed in our samples were treated as the background dataset.

Analysis of mRNA sequencing data

Raw reads of mRNA sequencing were first trimmed for adaptors and low-quality bases using Trimmomatic v0.36 software (35). Clean reads were aligned to the human reference genome (GRCh38.p12), coupled with the comprehensive gene annotation file (GENCODEv31) using STAR v2.7.1a (36). Gene expression was then quantified by counting unique mapped fragments to exons by using the feature count function from the Subread package (37). Raw counts for each gene were normalized to fragments per kilobase of a transcript, per million mapped reads (FPKM)-like values. Only mRNAs with FPKM ≥ 1 in at least ten samples were kept for the rest analysis. We used the same pipeline described above for mRNA DE and PCA analysis. The differentially expressed mRNAs were defined as FDR < 0.05 and |log2(fold change)| ≥ 0.58. WGCNA was carried out for 12,069 mRNAs with the optimal threshold power of 12 according to a fit to the scale-free topology of the co-expression network (Supplementary Figure S4A). Thirteen mRNA modules were identified with the settings: *maxBlockSize* = 20000, *minModuleSize* = 100 and *mergeCutHeight* = 0.25. Furthermore, mRNA module-enriched TF analysis was performed with a manually curated TF-target regulatory relationship database, TRRUST v2 (38), using Fisher's exact tests. TFs with FDR < 0.05 and odds ratio > 1 and the expression significantly correlated with respective mRNA modules (Pearson correlation *P-value* < 0.05) were identified.

<u>*Gene ontology (GO) analysis*</u> We carried out GO analysis for mRNAs by using the WebGestalt tool (http://www.webgestalt.org/) (39), which applied a hypergeometric test in target and reference gene sets. GO terms of non-redundant biological process (BP) with gene number less than 10 and adjust *P-value* (FDR) > 0.05 were filtered out.

Integrative analysis of miRNA and mRNA expression changes in wound healing

Expression correlation between mRNA and miRNA modules An integrative analysis was carried out by relating the first principal component (PC1) of miRNA expression, calculated using the *moduleEigengenes* function of WGCNA package (30), to the PC1 of mRNA expression in each module. The miRNA-mRNA module pairs with a Pearson correlation coefficient < -0.5 and a *P-value* < 0.05 were selected for the following enrichment analysis.

Prediction of miRNA targets We predicted both conserved and non-conserved target sites for all the 562 miRNAs by using the *get_multimir* function from R package multimiR (40) (http://multimir.org/) based on the latest TargetScan v7.2 database (41,42). All predicted miRNA targets were sorted by a primary score calculated for target site strength, and the top 25% with summed context++ score ≤ -0.15 were defined as the strongest miRNA targets. Targets that were not detected by the long RNA-seq were removed.

Gene set enrichment analysis of miRNA targets in mRNA modules. We evaluated the degree of enrichment of miRNA modules' targets in mRNA modules. For this, we focused on the VU-specific DE miRNA, i.e., the 22 up- and 10 down-regulated miRNAs in VU compared to both the skin and acute wounds (FDR < 0.05 and |log2(fold change)| ≥ 1), as well as the VU-associated modules' hub miRNAs, which kME values were greater than the median kME in respective modules (i.e., 14 miRNAs in m8, 9 miRNAs in m12, 20 miRNAs in m7, 29 miRNAs in m3, and 13 miRNAs in m9). Among these miRNAs' strongest targets, we selected the ones that were hit by ≥ 2 miRNAs from m8, m9, m12 modules or miRNAs downregulated in VU; ≥ 3 miRNAs from m7 module or miRNAs upregulated in VU; ≥ 4 miRNAs from m3 module, to capture putative module-driving targets. We performed gene set enrichment analyses for these miRs' targets in VU-specific DE mRNAs (FDR < 0.05 and fold change ≥ 1.5) and VU-associated mRNA modules by using the R function *fisher.test()* based on the two-side Fisher's exact test (43). Furthermore, we performed enrichment analysis to identify individual miRNA with their strongest targets significantly enriched in VU-specific DE mRNAs or VU-associated mRNA modules (Fisher's exact test: odds ratio > 1, *P-value* < 0.05).

Experimental validation of miRs' expression, targetome, and functions

Quantitative RT-PCR To detect miRNA, RNA from human skin and wounds was reverse transcribed using TaqMan® Advanced miRNA cDNA Synthesis Kit (Thermo Fisher Scientific). Individual miRNA expression was then quantified using TaqMan® Advanced miRNA Assays (Thermo Fisher Scientific) and normalized with miR-361-5p and miR-423-5p due to their relatively constant expression between human skin and wounds. To detect mRNA, we performed reverse transcription using the RevertAid First Strand cDNA Synthesis Kit (ThermoFisher Scientific). Gene expression was examined by SYBR Green expression assays (ThermoFisher Scientific) and normalized with housekeeping gene B2M and GAPDH. The primer sequences for B2M are forward primer (5'-AAGTGGGATCGAGACATGTAAG-3') and reverse primer (5'-GGAGACAGCACTCAAAGTAGAA-3'); GAPDH forward primer (5'-GGTGTGAACCATGAGAAGTATGA-3') and reverse primer (5'-GAGTCCTTCCACGATACCAAAG-3').

Primary cell culture and transfection Adult human epidermal keratinocytes were cultured in EpiLife serum-free keratinocyte growth medium supplemented with Human Keratinocyte Growth Supplement (HKGS) and 100 units/mL Penicillin and 100 µg/mL Streptomycin (Thermo Fisher Scientific). Adult human dermal fibroblasts were cultured in Medium 106 supplemented with Low Serum Growth Supplement (LSGS) and 100 units/mL Penicillin and 100 µg/mL Streptomycin (Thermo Fisher Scientific). Cells were incubated at 37°C in 5% CO_2, and media was routinely changed every 2-3 days. Third passage keratinocytes at 50%-60% confluence were transfected with 20 nM miRNA mimics (Horizon) or negative control using Lipofectamine™ 3000 (Thermo Fisher Scientific).

Microarray analysis Transcriptome profiling of keratinocytes and fibroblasts transfected with 20 nM miRNA mimics or control mimics for 24 hours (in triplicates) was performed using Affymetrix Genechip system at the Microarray Core facility of Karolinska Institute. Normalized expression data (log2 transformed value) were exported from Transcriptome Analysis Console (TAC) software and analyzed by the *limma* R package (44). In brief, expression data were first fitted to a linear model for each probe. Then, the empirical Bayes method was applied to compute the estimated coefficients of gene-wise variability and standard errors for comparisons of experimental and control groups. Genes with FC > 1.2 and *P*-value < 0.05 between the miRNA mimics- and the control mimics-transfected cells were considered to be significantly changed. Gene set enrichment analysis, including biological process (BP), Kyoto Encyclopedia of Genes and Genomes (KEGG) pathway, and hallmark from Molecular Signatures Database (MSigDB) (http://www.gsea-msigdb.org/) (45), was performed with a ranked fold change list

of all the genes by using the *fgsea* R package (46) and visualized by using the *ggplot2* (28) and *circlize* (47) packages.

Immunofluorescence staining Cells transfected with a combination of miRNA and/or control mimics (50 nM in total) were fixed in 4% paraformaldehyde (PFA) for 15 minutes. Cells were incubated with the Ki-67 antibody (Cell Signaling Technology) overnight at 4°C. The next day, cells were incubated with the secondary antibody conjugated with Alexa 488 for 40 minutes at room temperature. Cells were mounted with the ProLong™ Diamond Antifade Mountant with 4',6-Diamidino-2-Phenylindole (DAPI) (ThermoFisher Scientific). Ki-67 signals were visualized with Nikon microscopy, and positive cells were counted using ImageJ software (National Institutes of Health).

Cell proliferation assay Cells were seeded in 12-well plates with a density of 20,000 cells/well. The plates were placed in IncuCyte live-cell imaging and analysis platform (Essen Bioscience) after cells attaching to the plates. Plates were imaged every two hours, and pictures were processed and analyzed using IncuCyte ZOOM 2018A software (Essen Bioscience).

Statistical analysis Sample size of each experiment is indicated in the figure legend. Data analysis was performed by using R and Graphpad Prism 7 software. Comparison between two groups was performed with Mann-Whitney U tests (unpaired, non-parametric), Wilcoxon signed-rank test (paired, non-parametric), or two-tailed Student's t-test (parametric). The cell growth assay was analyzed by using two-way ANOVA. P-value < 0.05 is considered to be statistically significant.

RESULTS

miRNA and mRNA paired expression profiling in human wounds

To better understand tissue repair in humans, we collected wound-edge tissues from human acute wounds and chronic non-healing VUs (Figure 1A and Supplementary Tables S1–3). We created 4mm full thickness punch wounds at the lower legs of healthy volunteers aged beyond 60 years to match the advanced age of VU patients and anatomical location of the highest VUs occurrence (3). Tissue was collected at baseline (Skin), and at day one and day seven post-wounding (Wound1 and Wound7) to capture the inflammatory and proliferative phases of wound healing, respectively. In total, 20 samples divided into four groups, i.e., Skin, Wound1, Wound7, and VU, were analyzed by Illumina small RNA sequencing (sRNA-seq) and ribosomal RNA-depleted long RNA sequencing (RNA-seq). After stringent raw sequencing data quality control (Supplementary Tables S4-5), we detected 562 mature miRs and 12,069 mRNAs in our samples. Our principal component analysis showed that either the miR or the mRNA expression profiles clearly separated these four sample groups (Figure 1B). Next, we performed pairwise comparisons to identify the differentially expressed genes (DEG) during wound repair. We compared the VUs with both the skin and acute wounds and unraveled a VU-specific gene signature, including aberrant increase of 22 miRs and 221 mRNAs and decrease of 10 miRs and 203 mRNAs (DE analysis FDR < 0.05, fold change ≥ 2 for miRs and ≥ 1.5 for mRNAs, Figure 1C–E and Supplementary Table S6). The full DEG list can be browsed on our resource website (http://130.229.28.87/shiny/miRNA_Xulab/) with more or less rigorous cut-offs. With this unique resource, we dissected further the miR-mediated posttranscriptional regulatory underpinnings of wound repair.

Dynamically changed miR expression during wound repair

We leveraged weighted gene co-expression network analysis (WGCNA) for classifying miRs according to their co-expression patterns in the 20 sRNA-seq-analyzed samples to link the miR expression changes with wound healing progression or non-healing status at a system level (30). We identified 13 distinct modules with a robustness confirmed by the module preservation analysis (Supplementary Figure S1A), ten of them significantly correlating (Pearson's correlation, FDR < 0.05) with at least one of the four phenotypic traits, i.e., Skin, Wound1, Wound7, and VU (Figure 2A and B, Supplementary Table S7). The WGCNA revealed that module (m)2, m10, and m11 miRs were

upregulated at the inflammatory phase (Wound1), while m5 and m6 miRs peaked at the proliferative phase (Wound7). In VU, we identified three downregulated (m3, m7, and m9) and two upregulated (m8 and m12) miR modules. We highlighted the 198 "driver" miRs (i.e, the top 20 miRNAs with the highest kME values in each module and kME > 0.5) of the ten significant modules in the co-expression networks (Figure 2C and D and Supplementary Figure S2B–I) and they could also be browsed on our resource web portal (http://130.229.28.87/shiny/miRNA_Xulab/). Notably, we identified 84% of them as DEGs, suggesting a high consistence between the WGCNA and DE analysis (Supplementary Table S8).

We hypothesized that the co-expression of various miRs could be due to their transcription driven by common transcription factors (TF). To test this idea, we leveraged TransmiR v2.0 (34), a database including literature-curated and ChIP-seq-derived TF-miR regulation data, to identify the enriched TFs in each miR module [Fisher's extract test: odds ratio (OR) > 1, *FDR* < 0.05, Supplementary Table S9]. Interestingly, the BMP4, KLF4, KLF5, GATA3, GRHL2, and TP53 families exhibited not only their binding sites enriched in the m9 miR genes but their expression also significantly correlated with the m9 miRs (Pearson's correlation coefficient = 0.53–0.82, *P*-value of p = 7.05e-06–0.014) (Figure 2D, Supplementary Figure S3A and Table S9). Notably, the BMP4, GATA3, and KLF4 expressions were significantly reduced in VU compared to the skin and acute wounds. This result could explain the deficiency of their regulated miRs in VU and also suggest a link between these TFs and chronic wound pathology (Supplementary Figure S3B).

mRNA co-expression networks underpinning wound repair

miRs exert functions through the posttranscriptional regulation of their target mRNAs. Therefore, describing the mRNA expression context would be required for understanding the role of miRs in wound repair (42). We thus performed WGCNA in the paired long RNA-seq data and identified 13 mRNA co-expression modules (Figure 2E, Supplementary Figures S1B and S4A–C, and Table S10). The GO analysis of the mRNA modules largely confirmed the previous knowledge of wound biology, such as skin hemostasis (M2) and barrier function (M4)-related gene downregulation in the wounds, the upregulation of the genes involved in the immune response (M8), RNA processing, and protein production (M1, M3, and M5) in the inflammatory phase, and the prominent cell mitosis-related gene expression (M7) in the proliferative phase of wound repair (Figure 2F, Supplementary Figure S5A). These results further supported the robustness and reproducibility of our profiling data. Moreover, this

unique dataset allows the identification of the key TFs driving these biological processes. For example, we identified NFKB1 and RELA, well-known for their immune functions (48), as the most enriched upstream regulators for the M1 mRNAs, while E2F1, a TF promoting cell growth (49), surfaced as a master regulator TF in M7 (Supplementary Table S11).

Importantly, our study unraveled a VU molecular signature: downregulated expression of RNA and protein production- (M1, M3, and M5) as well as cell mitosis-related (M7) genes, and upregulated expression of genes involved in extracellular matrix organization and cell adhesion (M9). These results were in line with the dermal tissue fibrosis observed in patients with chronic venous insufficiency (50-52). Moreover, we found an immune gene signature clearly distinguishing the chronic inflammation in VUs (M11 and M12 enriched with adaptive immunity-related mRNAs) from the self-limiting immune response in acute wounds (M8 enriched with neutrophil activation- and phagocytosis-related mRNAs) (Figure 2F, Supplementary Figure S5B). Overall, we generated a gene expression map of human healing and non-healing wounds, setting a stepping stone for the in-depth understanding of the VU pathological mechanisms. After having established this map, we decided to dissect how miRs contribute to these pathological changes.

Integrative analysis of miR and mRNA expression changes in wound healing

Among the multiple gene expression regulatory mechanisms, we aimed to evaluate how miRs could contribute to the protein-coding gene expression in human wound repair. We thus performed a correlation analysis for the miRs and mRNAs that were differentially expressed in VU compared to the skin and acute wounds, using the first principal component (PC1) of their expression in each sample. We found significantly negative correlations (Pearson's correlation, P-values: 1.36e-12–1.27e-04) between the PC1 of the DE miRs and the DE mRNAs predicted as miR targets, indicating negative regulation of VU-mRNA signature by the aberrantly expressed miRs in VU (Figure 3A–C).

Furthermore, we dissected the potential regulatory relationship between the VU-associated miR and mRNA modules. We identified significantly negative correlations between the downregulated miR (m3, m7, and m9) and the upregulated mRNA (M9, M11, and M12) modules, as well as between the upregulated miR (m8 and m12) and the downregulated mRNA (M5) modules in VU (Figure 3D). Among these miR-mRNA module pairs, we found that the predicted targets of the downregulated m9 miRs were significantly enriched (Fisher's extract test: OR > 1, *P*-value < 0.05) for the upregulated M9

mRNAs, whereas the targets of the upregulated miRs and m8 miRs were enriched for the downregulated mRNAs and M5 mRNAs (Figure 4A, Supplementary Table S12). These results demonstrated that miRs significantly contribute to the aberrant mRNA expression in VU at a global level. Based on the above-identified miR-mRNA module pairs, we next searched for individual candidate miRs with their targets enriched for the VU mRNA signature. We observed that the targets of two VU-associated downregulated miRs (miR-144-3p and miR-218-5p) and five m9 miRs (miR-205-5p, miR-211-5p, miR-506-3p, miR-509-3p, and miR-96-5p) were enriched for the upregulated M9 mRNAs, whereas the targets of three VU-associated upregulated miRs (miR-450-5p, miR-512-3p, and miR-516b-5p) and seven m8 miRs (miR-424-5p, miR-34a-5p, miR-34c-5p, miR-516a-5p, miR-517a-3p, miR-517b-3p, and miR-7704) were enriched for M5 mRNAs and downregulated mRNAs (Figure 4B, Supplementary Table S13). These miR targetomes were enriched for the mRNAs associated with VU pathology. Therefore, these miR candidates are of importance for understanding the pathological mechanisms hindering wound healing. Moreover, we compiled miR-mediated gene expression regulation networks centered with these highly pathologically relevant miRs (Figure 4C, Supplementary Figures S6 and S7, and Table S13). These networks also include the mRNAs predicted as the strongest targets and with anti-correlated expression patterns with these miRs in human wounds *in vivo*, as well as the TFs reported to regulate these miR expressions from the TransmiR v2 database (34). Taken together, our study identifies a list of highly pathological relevant miRs and their targetomes in human VU.

Experimental validation of miR expressions and targets in human skin wounds

We selected nine shortlisted DE miRs (Figures 1D and 4B), including three downregulated (miR-149-5p, miR-218-5p, and miR-96-5p) and six upregulated (miR-7704, miR-424-5p, miR-31-3p, miR-450-5p, miR-516b-5p, and miR-517b-3p) miRs in VU, and validated their expression by qRT-PCR in a cohort with seven healthy donors and twelve VU patients, matched in terms of age and the anatomical wound locations (Supplementary Tables S2 and S3). We confirmed their expression patterns in RNA-seq, supporting the robustness and reproducibility of our profiling data (Figure 5A–I and Supplementary Figure S8).

Furthermore, we experimentally validated the targets of eight miRs surfaced in our analysis (Figure 4B), including the miRs downregulated (miR-218-5p and miR-96-5p) and upregulated (miR-424-5p, miR-

450-5p, miR-516b-5p, miR-34a-5p, miR-34c-5p, and miR-7704) in VU. We performed genome-wide microarray analysis in human primary keratinocytes or fibroblasts overexpressing each of these miRs. Furthermore, we re-analyzed our published microarray dataset on keratinocytes with miR-34a-5p or miR-34c-5p overexpression (GSE117506) (53). For all these eight miRs, we observed that their strongest targets predicted by TargetScan were significantly downregulated compared to the non-targeting mRNAs (Wilcoxon t-test P-values: 1.34e-25~1.91e-59). The differences were more significant when we divided the strongest targets into conserved and experimentally validated subtypes, confirming the bioinformatics prediction robustness of the miR targets applied in this study (Figure 5J–M and Supplementary Figure S9A–I).

Notably, we observed significant enrichment (Fisher's exact test, OR > 1, *P*-value < 0.05) of the experimentally validated miR-218-5p, miR-34a-5p, miR-34c-5p, and miR-7704 targets for the VU gene signature (Figure 5N, Supplementary Table S14). We have previously shown that miR-34a and miR-34c inhibit keratinocyte proliferation and migration, while promoting apoptosis and inflammatory response, resulting in delayed wound repair in a mouse model (53). We validated robustness of the bioinformatics approach applied in this study by miR-34a/c re-identification. Here, we discovered that both the predicted (Figure 4B) and validated (Figure 5N) miR-34a/c targets were enriched for the downregulated M5 module mRNAs in VU. Notably, our microarray analysis confirmed that miR-34a/c reduced the expression of 39 hub genes in the M5 module [log2(fold change) ≤ -0.58, *P*-value < 0.05, Supplementary Figure S9J], and 26 of them exhibited negative correlation (Pearson's $r = -0.83 – -0.45$, *P*-value < 0.05) with miR-34a/c expression levels in the human skin and wound samples (Figure 5O and Supplementary Table S14), suggesting that they were miR-34a/c targets *in vivo*. MiR-218-5p was downregulated in the VU compared to the acute wounds and the skin (Figure 5B, Supplementary Figure S8). Its predicted (Figure 4B) and validated (Figure 5N) targets were both enriched for the upregulated or M9 module mRNAs in VU. Among the ten *in vitro* validated targets, eight negatively correlated (Pearson's $r = -0.82 \sim -0.46$, *P*-value of $p < 0.05$) with miR-218-5p expression in the human skin and wounds (Figure 5O, Supplementary Figure S9J, and Table S14). Interestingly, this study also identified miR-7704, a human-specific miR, with significantly increased expression in VU (Figure 5D and Supplementary Figure S8). Similar to miR-34a/c, the predicted (Figure 4B) and validated (Figure 5N) miR-7704 targets were highly enriched for the M5 module mRNAs downregulated in VU.

For miR-96-5p, miR-424-5p, miR-450-5p, and miR-516b-5p, although their predicted targets were significantly enriched (Fisher's exact test: OR > 1, *P*-value < 0.05) for VU-associated mRNAs (Figure 4B), we did not find similar enrichment for their experimentally validated targets. Nevertheless, these miRs regulated some VU-associated hub genes *in vitro* (Supplementary Figure S9K) and also exhibited an anti-correlated expression pattern with their targets *in vivo* (Figure 5P), e.g., miR-96-5p from the downregulated m9 module targets the M9 mRNAs upregulated in VU, including TP53INP1, LAMC1, EDNRA, GJC1, and FN1; while miR-424-5p from the upregulated m8 miR module targets the M5 mRNAs downregulated in VU, including SLC25A22, VPS4A, and GHR (Supplementary Table S14).

In summary, we experimentally validated the expression and targets of the miRs identified by the RNA-seq data bioinformatics analysis, confirming the robustness and reproducibility of this dataset and highlighting its value as a reference for studying the physiological and pathological roles of miRs in human skin wound healing.

Cooperativity of VU pathology-relevant miRs

From the miR-mediated gene expression regulation networks underpinning VU pathology (Supplementary Figures S6 and S7, Table S13), we caught a glimpse of presumable miR cooperativity through targeting the same mRNAs, i.e., co-targeting among miRs, which reportedly imposing stronger and more complex repression patterns on target mRNA expression (54). For the miRs with unrelated seed sequences, we found that miR-34a/c and miR-424-5p or miR-7704 shared eight–ten targets, and these miRs were co-expressed in the m8 module. We showed that among the downregulated miRs in VU, miR-96-5p and miR-218-5p shared eight targets.

In addition, we performed functional annotations for the genes regulated by the VU-associated miRs identified in the microarray analysis (Figure 6A, Supplementary Table S15). Both miR-218-5p and miR-96-5p promoted ribosome biogenesis and non-coding (nc) RNA processing, while miR-218-5p also suppressed keratinization. miR-34a/c-5p enhanced innate immune response, while reducing mitosis. Similarly, miR-424-5p and miR-516b-5p increased the cellular defense response, while inhibiting cell proliferation. In addition, we showed that miR-450-5p upregulated genes related to the ncRNA metabolic process and mitochondrial respiratory chain complex assembly, whereas miR-7704 downregulated insulin, ERBB, and small GTPase-mediated signaling pathway-related genes. Of particular interest, combining the miR expression changes with their annotated functions, we found a

regular pattern, i.e., the miRs upregulated in VU (i.e., miR-34a-5p, miR-34c-5p, miR-424-5p, miR-450-5p, miR-7704, and miR-516-5p) promoted inflammation but inhibited proliferation; whereas the miRs downregulated in VU (i.e., miR-218-5p and miR-96-5p) were required for cell growth and activation (Figure 6B). Therefore, these VU-dysregulated miRs might cooperatively contribute to the stalled wound healing characterized with failed transition from inflammation-to-proliferation (55).

Cooperation of miR-34a, miR-424, and miR-516 in regulating keratinocyte proliferation and inflammatory response

To validate miR cooperativity in modulating the key pathological processes in VU, we analyzed proliferation and inflammatory response of keratinocytes overexpressing individual miR or miR combinations. The microarray data gene ontology analysis (Figure 6B) showed that three miRs upregulated in VU could suppress the expression of mitotic spindle-related genes (Figure 6C): miR-34a/c-5p reduced the level of 41 mRNAs (including two miR-34a/c targets), while miR-424-5p downregulated the expression of 67 mRNAs (including 14 miR-424 targets). Although 33 mRNAs were commonly regulated by miR-34a/c-5p and miR-424-5p, none of them were co-targeted by these miRs (Figure 6C). Similarly, in the cell cycle pathway, miR-34a-5p directly targeted CCND1, CDK6, HDAC1, and E2F3, while miR-424-5p targeted ANAPC13, CCNE1, CDC25B, CDK1, CDKN1B, CHK1, WEE1, and YWHAH, and only CDC23 was co-targeted by both miRs (Figure 7A). We thus hypothesized that miR-34a-5p and miR-424-5p might cooperate to impact stronger on cell proliferation by targeting different gene sets within the same signaling pathway. To test this idea, we measured keratinocyte growth by detecting proliferation marker gene Ki67 expression both on mRNA and protein levels. We found that although miR-34a-5p or miR-424-5p alone could reduce Ki67 levels, their combination suppressed stronger Ki67 expression (Figures 7B and C, Supplementary Figure S10A). The cooperativity between miR-34a-5p and miR-424-5p in repressing keratinocyte growth was further confirmed by comparing cell growth curves generated with a live cell imaging system (Figure 7D, Supplementary Figure S10B, Movie S1). Moreover, our microarray analysis showed that the miR-34a-5p and miR-516b-5p combination extended the list of inflammatory response-related upregulated genes (Figure 6D). In line with this, simultaneously overexpressing miR-34a-5p and miR-516b-5p induced a higher inflammatory chemokine CCL20 expression compared to the individual overexpression of each miRNA (Figure 7E). In summary, our study identified VU signature miRs, e.g., miR-34a, miR-424, and

miR-516, with cooperativity in inflicting more severe pathological changes (Figure 7F). These findings open new opportunities of developing wound treatment targeting cooperating miRs with potentially higher therapeutic efficacy and specificity.

DISCUSSION

Our genome-wide paired analysis of miR and mRNA expression in human healing and non-healing wounds provides a novel global landscape of the miR regulatory roles in wound biology. A detailed overview of the mRNA expression context at different healing stages or under pathological condition VU allows a more precise understanding about the complex role of miRs in wound repair. The same miR is often described to play different or even opposite roles in different cells, as each cell type has specific gene expression context subjected to the miR-mediated posttranscriptional regulation (56). Thereby, the different mRNA expression profiles in acute or chronic wounds should be considered to understand the precise role of an miR in these distinct contexts. With this aspect in mind, we highlight miRs with their targetome most enriched in the VU mRNA signature, as these miRs display a higher likelihood to regulate pathologically relevant genes. Notably, certain of these miRs did not exhibit the greatest expression change in VU, they would thus be missed with the commonly used strategy that focuses on the top miR expression profiling data changes.

Another strength of our study is the decryption of time-resolved miR-mRNA expression pattern during human skin wound healing, providing a temporal view to our understanding of the functional miR roles. miRs and their target gene expression contexts change dynamically to support different functional needs during wound repair. Defining an miR as “pro-healing” or “anti-healing” requires specifying its temporal expression pattern. For example, continuous expression of a miR that is beneficial for one healing phase but not the other might also lead to deleterious effects.

To understand the molecular mechanisms underlying the miR co-expression patterns, we analyzed the enriched TFs for each miR module with experimentally validated TF-miR regulation data (34). This analysis led us to important TFs, such as BMP4 (57,58) and GATA3 (59,60) that play fundamental roles in skin development and postnatal remodeling, as well as KLF4, crucial for establishing skin barrier function (61). Notably, both GATA3 and KLF4 are reportedly downregulated in human VU (62,63). Our study confirms these findings and provides a novel insight, showing that the loss of these TFs might contribute to VU pathology through their regulated miRs.

Numerous miRs that reportedly regulate wound healing in animal models also surfaced in our study, supporting the robustness of our profiling data and bioinformatics analysis. Thereby, our data would be potentially helpful to evaluate the clinical relevance of these miRs. For example, miR-34a/c reportedly

enhance keratinocyte inflammatory response, while suppressing proliferation and migration in cultured cells and mouse wound models (64). miR-34a was also identified as one of the most induced miRs in diabetic foot ulcer fibroblasts. Induction of miR-34a together with miR-21-5p and miR-145-5p inhibits fibroblast movement and proliferation, whereas activates cell differentiation and senescence (15). In this study, we described that miR-34a/c were specifically upregulated in VU, whereas their levels during wound repair remained relatively low and stable, suggesting their specific role in wound pathology. miR-34 targets were enriched in the M5 mRNA module, containing genes upregulated in the inflammatory phase of wound healing but downregulated in VUs. The VU-relevant miR-34 targetome identified in this study would be potentially useful for determining the precise role of miR-34 in VU pathology. Our current findings in human samples together with previous functional data (15,64) suggest that miR-34 inhibition along with modulation of additional deregulated miRs might be a promising VU treatment approach.

In addition, certain of these VU-related miRs are involved in skin-related functions but have not yet been linked to wound healing. For example, miR-218-5p regulates hair follicle development (65), inhibits melanogenesis (66), and enhances fibroblast differentiation (67). miR-7704 was identified as an exosomal miR produced by melanocytes (68). miR-424-5p suppresses keratinocyte proliferation (69) and cutaneous angiogenesis (70,71). Moreover, our VU-related miR list (Figure 4B) also contains miRs without prior knowledge in their role either in skin or wound healing, e.g., miR-517a-3p, miR-517b-3p, miR-516b-5p, miR-512-3p, and miR-450-5p. It would be highly interesting to examine the role of these miRs in VU. Overall, our dataset can serve as a valuable reference for prioritizing clinically relevant miRs for further functional studies.

Moreover, we studied the relationships between the dysregulated miRs in VU, regarding their target repertoire and biological functions and identified miRs that could act cooperatively. Such knowledge is required for developing combined miR therapeutics with increased specificity and efficacy (72). In the miR-target networks underpinning VU (Supplementary Figure S6 and S7), we identified a few putative cooperating miR pairs/clusters that were co-expressed and shared multiple common targets, including the upregulated miR-34 a/c together with miR-424-5p and miR-7704, as well as the downregulated miR-218-5p and miR-96-5p in VU. Furthermore, although not sharing targets, the majority of the VU-dysregulated miRs could still regulate the common biological processes coordinately. For example, the miRs upregulated in VU (e.g., miR-34a/c-5p, miR-424-5p, miR-450-5p, miR-7704, and miR-516-5p) promote inflammation but inhibit proliferation; whereas the miRs downregulated in VU (e.g., miR-218-

5p and miR-96-5p) are needed for cell growth and activation. As a combined consequence, this VU-miR signature could disrupt the swift transition from inflammation to proliferation (Figure 7F). The failure of this phase transition represents a core pathology of chronic wounds (2,55). Our findings open the possibility of developing innovative wound treatment targeting multiple pathologically relevant cooperating miRs to attain higher therapeutic efficacy and specificity.

A limitation of our study is the lack of cell type specific miR expression data. Certain gene expression changes detected in the tissue biopsies might be due to the changes of cellular compositions. To rule out this possibility, we validated miR-mediated gene regulation in individual skin cell types (i.e., keratinocytes and fibroblasts) for several miRs surfaced in our analysis. However, to systemically differentiate the gene expression regulation occurring in an individual cell from the altered cellular composition in wound tissues requires future studies using single-cell small RNA sequencing, which technology still remains challenging to be used at a scale for analyzing complex dynamics of tissue, such as human skin and wounds, as it needs extensive cell handing and therefore has only been applied to few cells (73). As new technologies for higher cellular resolution miRNA analyses emerge, we hope that such approach will be feasible in a near future.

In conclusion, this genome-wide, integrative analysis of miR and mRNA expression in human skin and wound tissues reinforce and extend the evidence about the functional role of miRs in wound repair and their therapeutic potential for chronic wound treatment. By combining miR expression patterns with their specific target gene expression context, we identified miRs highly relevant to VU pathology. This rigorous and in-depth molecular characterization of human wound tissues adds a novel dimension to our current knowledge mostly relying on non-human models and would serve as an unique platform and valuable resource for further mechanistic studies of miRs with a high translational potential.

DATA AVAILABILITY

Raw data of small RNA sequencing and long RNA sequencing performed in this study have been deposited to NCBI's Gene Expression Omnibus (GEO) database under the accession number GSE174661. The microarray data are available from the corresponding author upon reasonable request. In addition, the analyzed dataset is presented with an online R Shiny app and can be accessed through a browsable web portal (http://130.229.28.87/shiny/miRNA_Xulab/). The analysis source code is available at https://github.com/Zhuang-Bio/miRNAprofiling.

SUPPLEMENTARY DATA

Supplementary Data are available.

ACKNOWLEDGEMENT

We express our gratitude to the patients and healthy donors participating in this study. We thank Mona Ståhle, Desiree Wiegleb Edström, Peter Berg, Fredrik Correa, Martin Gumulka, Mahsa Tayefi for clinical sample collection; Helena Griehsel for technical support. We thank the Microarray core facility at Novum, BEA, which is supported by the board of research at KI and the research committee at the Karolinska hospital. The computations/data handling was enabled by resources in the projects sens2020010 and 2021/22-701 provided by the Swedish National Infrastructure for Computing (SNIC) at UPPMAX, partially funded by the Swedish Research Council through grant agreement no. 2018-05973.

Author contributions: N.X.L. and P.S. conceived and designed the study. P.S. collected most clinical samples with the assistance of M.A.T.. L.Z., D.L., M.A.T., and X.B. performed the experiments. Z.L. and L.Z. carried out bioinformatics analysis. I.P. and M.T.C contributed to data analyses and interpretation. Z.L., L.Z., and N.X.L. wrote the manuscript, which was commented on by all authors.

FUNDING

This work was supported by Swedish Research Council (Vetenskapsradet, 2016-02051 and 2020-01400), Ragnar Söderbergs Foundation (M31/15), Welander and Finsens Foundation (Hudfonden), LEO foundation, Ming Wai Lau Centre for Reparative Medicine, Karolinska Institutet, and R01AR073614 from NIH/NIAMS (to MTC).

CONFLICT OF INTEREST

The authors declare no conflict of interest.

FIGURE LEGENDS

Figure 1. Paired profiling of miRNA and mRNA expression in human wounds. (**A**) Schematic of analysis in this study. (**B**) PCA plots based on miRNA (upper panel) and mRNA (lower panel) expression profiles. Each dot indicates an individual sample. The numbers of differentially expressed (DE) miRNAs (**C**) and mRNAs (**E**) in VU (n=5) compared to the Skin, Wound1, and Wound7 from 5 healthy donors are shown in Venn diagrams. FDR < 0.05, fold change ≥ 2 for miRNAs and ≥ 1.5 for mRNAs. (**D**) The heatmap depicts the 32 miRNAs specifically dysregulated in the VU with scaled expression values (Z-scores). WGCNA modules of each miRNA belongs to are marked with color bars. The miRNAs with experimentally validated expression changes are highlighted in red.

Figure 2. Weighted gene co-expression network analysis (WGCNA) of miRNAs and mRNAs in wound healing. (**A**) Cluster dendrogram shows miRNA co-expression modules: each branch corresponds to a module, and each leaf indicates a single miRNA. Color bars below show the module assignment (the 1st row) and Pearson correlation coefficients between miRNA expression and the sample groups (the 2nd to the 5th row: red and blue lines represent positive and negative correlations, respectively). (**B**) Heatmap shows Pearson correlations between miRNA module eigengenes (ME) and the sample groups. The correlation coefficients and the adjusted *P-values* (FDR) are shown where the FDRs are less than 0.05. For the VU-associated modules m8 (**C**) and m9 (**D**), bar plots (left) depict the ME values across the 20 samples analyzed by RNA-seq, and network plots (right) show the top 20 miRNAs with the highest kME values in each module. Node size and edge thickness are proportional to the kME values and the weighted correlations between two connected miRNAs, respectively. The miRs with their targetome enriched with VU-mRNA signature (see Figure 4B) are highlighted in red. Transcription factors (TFs) with their targets enriched in the m9 module (Fisher's exact test: FDR < 0.05) are listed below the network, and TFs differentially expressed in VU are underlined. (**E**) Heatmap shows Pearson correlations between mRNA MEs and the sample groups. (**F**) The gene expression pattern of each module across all the sample groups is depicted with line charts. Gene ontology analysis of biological processes enriched in each module is shown at the right.

Figure 3. Correlation analysis between miRNA and mRNA expression changes in VU. (**A-C**) Correlations between the first principal component (PC1) of VU-associated differentially expressed (DE)

miRNAs, and the PC1 of VU DE mRNAs predicted as miRNA targets. (**D**) PC1 correlations between the hub miRNAs and their predicted targets in the VU-associated miRNA and mRNA modules. Pearson correlation coefficients (*r*) and *P* values are shown. The mRNA networks are plotted with the top 20 most connected module genes. Transcription factors (TFs) with targets enriched in the VU-associated modules are listed below the networks.

Figure 4. Integrative analysis of miRNA and mRNA expression changes in VU. Heatmaps show the enrichment for VU-affected mRNAs and mRNA modules in the top targets of (**A**) VU-associated DE miRNAs and miR modules and (**B**) the individual candidate miRNAs. Odds ratio (OR) and *P* values are indicated when OR > 1 and *P-value* < 0.05 (Fisher's exact test). The miRNAs with experimentally validated expression changes are highlighted in bold. (**C**) miR-mediated gene regulatory networks in VU are constructed with the miRNAs in Figure 4B, the mRNAs predicted as the strongest targets and with anti-correlated expression patterns (Pearson correlation, *P-value* < 0.05 and r < 0) with these miRNAs in human wounds, and the TFs regulating these miRNAs' expression from the TransmiR v2 database. An enlarged version of these networks can be found in Supplementary Figures S6 and S7.

Figure 5. Experimental validation of miRNAs' expression and targets in human skin wounds. (**A-I**) qRT-PCR analysis of VU-associated DE miRNAs in the skin, day 1 and day 7 acute wounds from 7 healthy donors and venous ulcers (VU) from 12 patients. Wilcoxon signed-rank test was used for the comparison between Skin, Wound1, and Wound7; Mann-Whitney U test was used for comparing VU with the skin and acute wounds. **P* < 0.05, ***P* < 0.01, ****P* < 0.001, *****P* < 0.0001. (**J-M**) Microarray analysis was performed in keratinocytes (KC) with miR-218-5p (**J**), miR-34a-5p (**K**), miR-34c-5p (**L**), or miR-7704 (**M**) overexpression (OE), and density plots of mRNAs $\log_2$(fold change) are shown. Wilcoxon t-tests were performed to compare the TargetScan predicted strongest targets (purple) with the non-targets (blue) for each of these miRNAs. The conserved and experimentally validated targets are marked with red and green colors, respectively. Dotted lines depict the average log2(fold change) values for each mRNA group. (**N**) A heatmap shows the enrichment for VU-affected mRNAs and mRNA modules in the targets of miR-218-5p, miR-34a-5p, miR-34c-5p, or miR-7704 validated by the microarray analysis. Odds ratio (OR) and *P* values are shown when OR > 1 and *P-value* < 0.05 (Fisher's exact test). (**O, P**) For each of the miRNAs (miR-218-5p, miR-34a-5p, miR-34c-5p, miR-7704, miR-96,

miR-424, miR-450b, and miR-516b) and its targets validated by the microarray analysis of KC or fibroblasts (FB), Pearson correlation analysis was performed between their expression values in human skin and wound samples shown by RNA-seq. Grey circles indicate correlation coefficients > 0.

Figure 6. Cooperativity of VU pathology-relevant miRNAs. For the microarray data in keratinocytes (KC) or fibroblasts (FB) with miR-218-5p, miR-96-5p, miR-34a-5p, miR-34c-5p, miR-7704, miR-424-5p, miR-516-5p overexpression, we analyzed KEGG pathways, biological processes (**A**), and Molecular Signatures Database (MSigDB) hallmarks (**B**) enriched by the genes up-or down-regulated by these miRNAs. Venn diagrams show the numbers of the mitotic spindle-related genes regulated by miR-34a/c-5p and miR-424-5p (**C**) and the inflammatory response-related genes regulated by miR-34a/c-5p and miR-516b-5p (**D**) (fold change > 1.2, *P*-value < 0.05) in the microarray analysis of keratinocytes overexpressing these miRNAs. Among the regulated genes, the targets of each miRNA are depicted in the plots.

Figure 7. Cooperation of miR-34a, miR-424, and miR-516 in regulating keratinocyte proliferation and inflammatory response. (**A**) In the KEGG cell cycle pathway map, genes regulated by miR-34a-5p or miR-424-5p or both miRNAs as shown in the microarray analysis of keratinocytes are marked with green, blue, and orange colors, respectively. Among the regulated genes, the miRNA targets are highlighted in red and labeled with * for miR-34a targets, # for miR-424 targets, *# for the gene co-targeted by both miRNAs. Ki67 expression was detected in keratinocytes transfected with miR-34a-5p or miR-424-5p mimics alone or both mimics for 24 hours (n = 3) by qRT-PCR (**B**) and immunofluorescence staining (n = 5 for Ctl and miR-34a-5p/424-5p, n = 4 for miR-34a-5p/ctl and miR-424-5p/ctl) (**C**). (**D**) The growth of the transfected keratinocytes (n = 3) was analyzed with a live cell imaging system. (**E**) qRT-PCR analysis of CCL20 in keratinocytes transfected with miR-34a-5p or miR-516b-5p mimics alone or both mimics for 24 hours (n = 3). (**F**) Proposed mechanism by which VU-dysregulated miRNAs cooperatively contribute to the stalled wound healing characterized with failed inflammation-proliferation transition. *$P < 0.05$; **$P < 0.01$; ***$P < 0.001$ and ****$P<0.0001$ by unpaired two-tailed Student's t-test (**B, C,** and **E**) and Two-way ANOVA (**D**). Data are presented as mean ± SD.

REFERENCES

1. Reinke, J.M. and Sorg, H. (2012) Wound repair and regeneration. *European surgical research. Europaische chirurgische Forschung. Recherches chirurgicales europeennes*, **49**, 35-43.
2. Eming, S.A., Martin, P. and Tomic-Canic, M. (2014) Wound repair and regeneration: mechanisms, signaling, and translation. *Sci Transl Med*, **6**, 265sr266.
3. Vivas, A., Lev-Tov, H. and Kirsner, R.S. (2016) Venous Leg Ulcers. *Ann Intern Med*, **165**, Itc17-itc32.
4. Hoversten, K.P., Kiemele, L.J., Stolp, A.M., Takahashi, P.Y. and Verdoorn, B.P. (2020) Prevention, Diagnosis, and Management of Chronic Wounds in Older Adults. *Mayo Clin Proc*, **95**, 2021-2034.
5. Stone, R.C., Stojadinovic, O., Rosa, A.M., Ramirez, H.A., Badiavas, E., Blumenberg, M. and Tomic-Canic, M. (2017) A bioengineered living cell construct activates an acute wound healing response in venous leg ulcers. *Sci Transl Med*, **9**.
6. Stavast, C.J. and Erkeland, S.J. (2019) The Non-Canonical Aspects of MicroRNAs: Many Roads to Gene Regulation. *Cells*, **8**, 1465.
7. Meng, Z., Zhou, D., Gao, Y., Zeng, M. and Wang, W. (2018) miRNA delivery for skin wound healing. *Adv Drug Deliv Rev*, **129**, 308-318.
8. Herter, E.K. and Xu Landén, N. (2017) Non-Coding RNAs: New Players in Skin Wound Healing. *Adv Wound Care (New Rochelle)*, **6**, 93-107.
9. Peak calling ChIP-seq/ATAC-seq data using MACS2.
10. Rupaimoole, R. and Slack, F.J. (2017) MicroRNA therapeutics: towards a new era for the management of cancer and other diseases. *Nat Rev Drug Discov*, **16**, 203-222.
11. Luan, A., Hu, M.S., Leavitt, T., Brett, E.A., Wang, K.C., Longaker, M.T. and Wan, D.C. (2018) Noncoding RNAs in Wound Healing: A New and Vast Frontier. *Adv Wound Care (New Rochelle)*, **7**, 19-27.
12. Nie, X., Zhao, J., Ling, H., Deng, Y., Li, X. and He, Y. (2020) Exploring microRNAs in diabetic chronic cutaneous ulcers: Regulatory mechanisms and therapeutic potential. *Br J Pharmacol*, **177**, 4077-4095.
13. Sen, C.K. and Roy, S. (2012) OxymiRs in cutaneous development, wound repair and regeneration. *Semin Cell Dev Biol*, **23**, 971-980.

14. Pastar, I., Marjanovic, J., Stone, R.C., Chen, V., Burgess, J.L., Mervis, J.S. and Tomic-Canic, M. (2021) Epigenetic regulation of cellular functions in wound healing. *Exp Dermatol*.

15. Liang, L., Stone, R.C., Stojadinovic, O., Ramirez, H., Pastar, I., Maione, A.G., Smith, A., Yanez, V., Veves, A., Kirsner, R.S. *et al.* (2016) Integrative analysis of miRNA and mRNA paired expression profiling of primary fibroblast derived from diabetic foot ulcers reveals multiple impaired cellular functions. *Wound Repair Regen*, **24**, 943-953.

16. Ramirez, H.A., Pastar, I., Jozic, I., Stojadinovic, O., Stone, R.C., Ojeh, N., Gil, J., Davis, S.C., Kirsner, R.S. and Tomic-Canic, M. (2018) Staphylococcus aureus Triggers Induction of miR-15B-5P to Diminish DNA Repair and Deregulate Inflammatory Response in Diabetic Foot Ulcers. *J Invest Dermatol*, **138**, 1187-1196.

17. Liang, P., Lv, C., Jiang, B., Long, X., Zhang, P., Zhang, M., Xie, T. and Huang, X. (2012) MicroRNA profiling in denatured dermis of deep burn patients. *Burns*, **38**, 534-540.

18. Li, D., Wang, A., Liu, X., Meisgen, F., Grünler, J., Botusan, I.R., Narayanan, S., Erikci, E., Li, X., Blomqvist, L. *et al.* (2015) MicroRNA-132 enhances transition from inflammation to proliferation during wound healing. *J Clin Invest*, **125**, 3008-3026.

19. Elliot, S., Wikramanayake, T.C., Jozic, I. and Tomic-Canic, M. (2018) A Modeling Conundrum: Murine Models for Cutaneous Wound Healing. *J Invest Dermatol*, **138**, 736-740.

20. Darwin, E. and Tomic-Canic, M. (2018) Healing Chronic Wounds: Current Challenges and Potential Solutions. *Curr Dermatol Rep*, **7**, 296-302.

21. Pastar, I., Wong, L.L., Egger, A.N. and Tomic-Canic, M. (2018) Descriptive vs mechanistic scientific approach to study wound healing and its inhibition: Is there a value of translational research involving human subjects? *Exp Dermatol*, **27**, 551-562.

22. Mackowiak, S.D. (2011) Identification of novel and known miRNAs in deep-sequencing data with miRDeep2. *Curr Protoc Bioinformatics*, **Chapter 12**, Unit 12 10.

23. Friedlander, M.R., Mackowiak, S.D., Li, N., Chen, W. and Rajewsky, N. (2012) miRDeep2 accurately identifies known and hundreds of novel microRNA genes in seven animal clades. *Nucleic Acids Res*, **40**, 37-52.

24. Langmead, B., Trapnell, C., Pop, M. and Salzberg, S.L. (2009) Ultrafast and memory-efficient alignment of short DNA sequences to the human genome. *Genome Biology*, **10**, R25.

25. Kozomara, A., Birgaoanu, M. and Griffiths-Jones, S. (2018) miRBase: from microRNA sequences to function. *Nucleic Acids Research*, **47**, D155-D162.

26. Zhou, L., Chen, J., Li, Z., Li, X., Hu, X., Huang, Y., Zhao, X., Liang, C., Wang, Y., Sun, L. *et al.* (2010) Integrated profiling of microRNAs and mRNAs: microRNAs located on Xq27.3 associate with clear cell renal cell carcinoma. *PLoS One*, **5**, e15224.

27. Love, M.I., Huber, W. and Anders, S. (2014) Moderated estimation of fold change and dispersion for RNA-seq data with DESeq2. *Genome Biology*, **15**, 550.

28. Hadley, W. (2016) ggplot2: Elegant Graphics for Data Analysis. *Springer-Verlag New York*.

29. Gu, Z., Eils, R. and Schlesner, M. (2016) Complex heatmaps reveal patterns and correlations in multidimensional genomic data. *Bioinformatics*, **32**, 2847-2849.

30. Langfelder, P. and Horvath, S. (2008) WGCNA: an R package for weighted correlation network analysis. *BMC Bioinformatics*, **9**, 559.

31. Zhang, B. and Horvath, S. (2005) A general framework for weighted gene co-expression network analysis. *Stat Appl Genet Mol Biol*, **4**, Article17.

32. Shannon, P., Markiel, A., Ozier, O., Baliga, N.S., Wang, J.T., Ramage, D., Amin, N., Schwikowski, B. and Ideker, T. (2003) Cytoscape: a software environment for integrated models of biomolecular interaction networks. *Genome Res*, **13**, 2498-2504.

33. Langfelder, P., Luo, R., Oldham, M.C. and Horvath, S. (2011) Is my network module preserved and reproducible? *PLoS Comput Biol*, **7**, e1001057.

34. Tong, Z., Cui, Q., Wang, J. and Zhou, Y. (2019) TransmiR v2.0: an updated transcription factor-microRNA regulation database. *Nucleic Acids Res*, **47**, D253-d258.

35. Bolger, A.M., Lohse, M. and Usadel, B. (2014) Trimmomatic: a flexible trimmer for Illumina sequence data. *Bioinformatics*, **30**, 2114-2120.

36. Dobin, A., Davis, C.A., Schlesinger, F., Drenkow, J., Zaleski, C., Jha, S., Batut, P., Chaisson, M. and Gingeras, T.R. (2013) STAR: ultrafast universal RNA-seq aligner. *Bioinformatics*, **29**, 15-21.

37. Liao, Y., Smyth, G.K. and Shi, W. (2013) featureCounts: an efficient general purpose program for assigning sequence reads to genomic features. *Bioinformatics*, **30**, 923-930.

38. Han, H., Cho, J.W., Lee, S., Yun, A., Kim, H., Bae, D., Yang, S., Kim, C.Y., Lee, M., Kim, E. *et al.* (2018) TRRUST v2: an expanded reference database of human and mouse transcriptional regulatory interactions. *Nucleic Acids Res*, **46**, D380-d386.

39. Liao, Y., Wang, J., Jaehnig, E.J., Shi, Z. and Zhang, B. (2019) WebGestalt 2019: gene set analysis toolkit with revamped UIs and APIs. *Nucleic Acids Research*, **47**, W199-W205.

40. Ru, Y., Kechris, K.J., Tabakoff, B., Hoffman, P., Radcliffe, R.A., Bowler, R., Mahaffey, S., Rossi, S., Calin, G.A., Bemis, L. *et al.* (2014) The multiMiR R package and database: integration of microRNA–target interactions along with their disease and drug associations. *Nucleic Acids Research*, **42**, e133-e133.

41. Lewis, B.P., Burge, C.B. and Bartel, D.P. (2005) Conserved Seed Pairing, Often Flanked by Adenosines, Indicates that Thousands of Human Genes are MicroRNA Targets. *Cell*, **120**, 15-20.

42. Agarwal, V., Bell, G.W., Nam, J.W. and Bartel, D.P. (2015) Predicting effective microRNA target sites in mammalian mRNAs. *Elife*, **4**.

43. Wu, Y.E., Parikshak, N.N., Belgard, T.G. and Geschwind, D.H. (2016) Genome-wide, integrative analysis implicates microRNA dysregulation in autism spectrum disorder. *Nat Neurosci*, **19**, 1463-1476.

44. Ritchie, M.E., Phipson, B., Wu, D., Hu, Y., Law, C.W., Shi, W. and Smyth, G.K. (2015) limma powers differential expression analyses for RNA-sequencing and microarray studies. *Nucleic Acids Research*, **43**, e47-e47.

45. Subramanian, A., Tamayo, P., Mootha, V.K., Mukherjee, S., Ebert, B.L., Gillette, M.A., Paulovich, A., Pomeroy, S.L., Golub, T.R., Lander, E.S. *et al.* (2005) Gene set enrichment analysis: a knowledge-based approach for interpreting genome-wide expression profiles. *Proc Natl Acad Sci U S A*, **102**, 15545-15550.

46. Korotkevich, G., Sukhov, V., Budin, N., Shpak, B., Artyomov, M.N. and Sergushichev, A. (2021) Fast gene set enrichment analysis. *bioRxiv*, 060012.

47. Gu, Z., Gu, L., Eils, R., Schlesner, M. and Brors, B. (2014) circlize Implements and enhances circular visualization in R. *Bioinformatics*, **30**, 2811-2812.

48. Liu, T., Zhang, L., Joo, D. and Sun, S.-C. (2017) NF-κB signaling in inflammation. *Signal Transduction and Targeted Therapy*, **2**, 17023.

49. Ertosun, M.G., Hapil, F.Z. and Osman Nidai, O. (2016) E2F1 transcription factor and its impact on growth factor and cytokine signaling. *Cytokine & Growth Factor Reviews*, **31**, 17-25.

50. Pappas, P.J., You, R., Rameshwar, P., Gorti, R., DeFouw, D.O., Phillips, C.K., Padberg, F.T., Jr., Silva, M.B., Jr., Simonian, G.T., Hobson, R.W., 2nd *et al.* (1999) Dermal tissue fibrosis in patients with chronic venous insufficiency is associated with increased transforming growth factor-beta1 gene expression and protein production. *J Vasc Surg*, **30**, 1129-1145.

51. Blumberg, S.N., Maggi, J., Melamed, J., Golinko, M., Ross, F. and Chen, W. (2012) A histopathologic basis for surgical debridement to promote healing of venous ulcers. *J Am Coll Surg*, **215**, 751-757.

52. Stone, R.C., Stojadinovic, O., Sawaya, A.P., Glinos, G.D., Lindley, L.E., Pastar, I., Badiavas, E. and Tomic-Canic, M. (2020) A bioengineered living cell construct activates metallothionein/zinc/MMP8 and inhibits TGFβ to stimulate remodeling of fibrotic venous leg ulcers. *Wound Repair Regen*, **28**, 164-176.

53. Pachera, E., Assassi, S., Salazar, G.A., Stellato, M., Renoux, F., Wunderlin, A., Blyszczuk, P., Lafyatis, R., Kurreeman, F., de Vries-Bouwstra, J. *et al.* (2020) Long noncoding RNA H19X is a key mediator of TGF-beta-driven fibrosis. *J Clin Invest*, **130**, 4888-4905.

54. Cherone, J.M., Jorgji, V. and Burge, C.B. (2019) Cotargeting among microRNAs in the brain. *Genome research*, **29**, 1791-1804.

55. Landén, N.X., Li, D. and Ståhle, M. (2016) Transition from inflammation to proliferation: a critical step during wound healing. *Cell Mol Life Sci*, **73**, 3861-3885.

56. Erhard, F., Haas, J., Lieber, D., Malterer, G., Jaskiewicz, L., Zavolan, M., Dölken, L. and Zimmer, R. (2014) Widespread context dependency of microRNA-mediated regulation. *Genome research*, **24**, 906-919.

57. Botchkarev, V.A. (2003) Bone Morphogenetic Proteins and Their Antagonists in Skin and Hair Follicle Biology. *Journal of Investigative Dermatology*, **120**, 36-47.

58. Lewis, C.J., Mardaryev, A.N., Poterlowicz, K., Sharova, T.Y., Aziz, A., Sharpe, D.T., Botchkareva, N.V. and Sharov, A.A. (2014) Bone morphogenetic protein signaling suppresses wound-induced skin repair by inhibiting keratinocyte proliferation and migration. *J Invest Dermatol*, **134**, 827-837.

59. Kaufman, C.K., Zhou, P., Pasolli, H.A., Rendl, M., Bolotin, D., Lim, K.C., Dai, X., Alegre, M.L. and Fuchs, E. (2003) GATA-3: an unexpected regulator of cell lineage determination in skin. *Genes Dev*, **17**, 2108-2122.

60. Kurek, D., Garinis, G.A., van Doorninck, J.H., van der Wees, J. and Grosveld, F.G. (2007) Transcriptome and phenotypic analysis reveals Gata3-dependent signalling pathways in murine hair follicles. *Development*, **134**, 261-272.

61. Segre, J.A., Bauer, C. and Fuchs, E. (1999) Klf4 is a transcription factor required for establishing the barrier function of the skin. *Nature Genetics*, **22**, 356-360.

62. Stojadinovic, O., Pastar, I., Vukelic, S., Mahoney, M.G., Brennan, D., Krzyzanowska, A., Golinko, M., Brem, H. and Tomic-Canic, M. (2008) Deregulation of keratinocyte differentiation and activation: a hallmark of venous ulcers. *J Cell Mol Med*, **12**, 2675-2690.

63. Stojadinovic, O., Pastar, I., Nusbaum, A.G., Vukelic, S., Krzyzanowska, A. and Tomic-Canic, M. (2014) Deregulation of epidermal stem cell niche contributes to pathogenesis of nonhealing venous ulcers. *Wound Repair Regen*, **22**, 220-227.

64. Wu, J., Li, X., Li, D., Ren, X., Li, Y., Herter, E.K., Qian, M., Toma, M.A., Wintler, A.M., Serezal, I.G. *et al.* (2020) MicroRNA-34 Family Enhances Wound Inflammation by Targeting LGR4. *J Invest Dermatol*, **140**, 465-476 e411.

65. Zhao, B., Chen, Y., Yang, N., Chen, Q., Bao, Z., Liu, M., Hu, S., Li, J. and Wu, X. (2019) miR-218-5p regulates skin and hair follicle development through Wnt/β-catenin signaling pathway by targeting SFRP2. *J Cell Physiol*, **234**, 20329-20341.

66. Guo, J., Zhang, J.F., Wang, W.M., Cheung, F.W., Lu, Y.F., Ng, C.F., Kung, H.F. and Liu, W.K. (2014) MicroRNA-218 inhibits melanogenesis by directly suppressing microphthalmia-associated transcription factor expression. *RNA Biol*, **11**, 732-741.

67. Guo, F., Carter, D.E. and Leask, A. (2014) miR-218 regulates focal adhesion kinase-dependent TGFβ signaling in fibroblasts. *Mol Biol Cell*, **25**, 1151-1158.

68. Shen, Z., Sun, J., Shao, J. and Xu, J. (2020) Ultraviolet B irradiation enhances the secretion of exosomes by human primary melanocytes and changes their exosomal miRNA profile. *PLoS One*, **15**, e0237023.

69. Ichihara, A., Jinnin, M., Yamane, K., Fujisawa, A., Sakai, K., Masuguchi, S., Fukushima, S., Maruo, K. and Ihn, H. (2011) microRNA-mediated keratinocyte hyperproliferation in psoriasis vulgaris. *Br J Dermatol*, **165**, 1003-1010.

70. Nakashima, T., Jinnin, M., Etoh, T., Fukushima, S., Masuguchi, S., Maruo, K., Inoue, Y., Ishihara, T. and Ihn, H. (2010) Down-regulation of mir-424 contributes to the abnormal angiogenesis via MEK1 and cyclin E1 in senile hemangioma: its implications to therapy. *PLoS One*, **5**, e14334.

71. Yang, L., Dai, J., Li, F., Cheng, H., Yan, D. and Ruan, Q. (2017) The expression and function of miR-424 in infantile skin hemangioma and its mechanism. *Sci Rep*, **7**, 11846.

72. Lai, X., Eberhardt, M., Schmitz, U. and Vera, J. (2019) Systems biology-based investigation of cooperating microRNAs as monotherapy or adjuvant therapy in cancer. *Nucleic Acids Research*, **47**, 7753-7766.

73. Nielsen, M.M. and Pedersen, J.S. (2020) miRNA activity inferred from single cell mRNA expression. *bioRxiv*, 2020.2007.2014.202051.

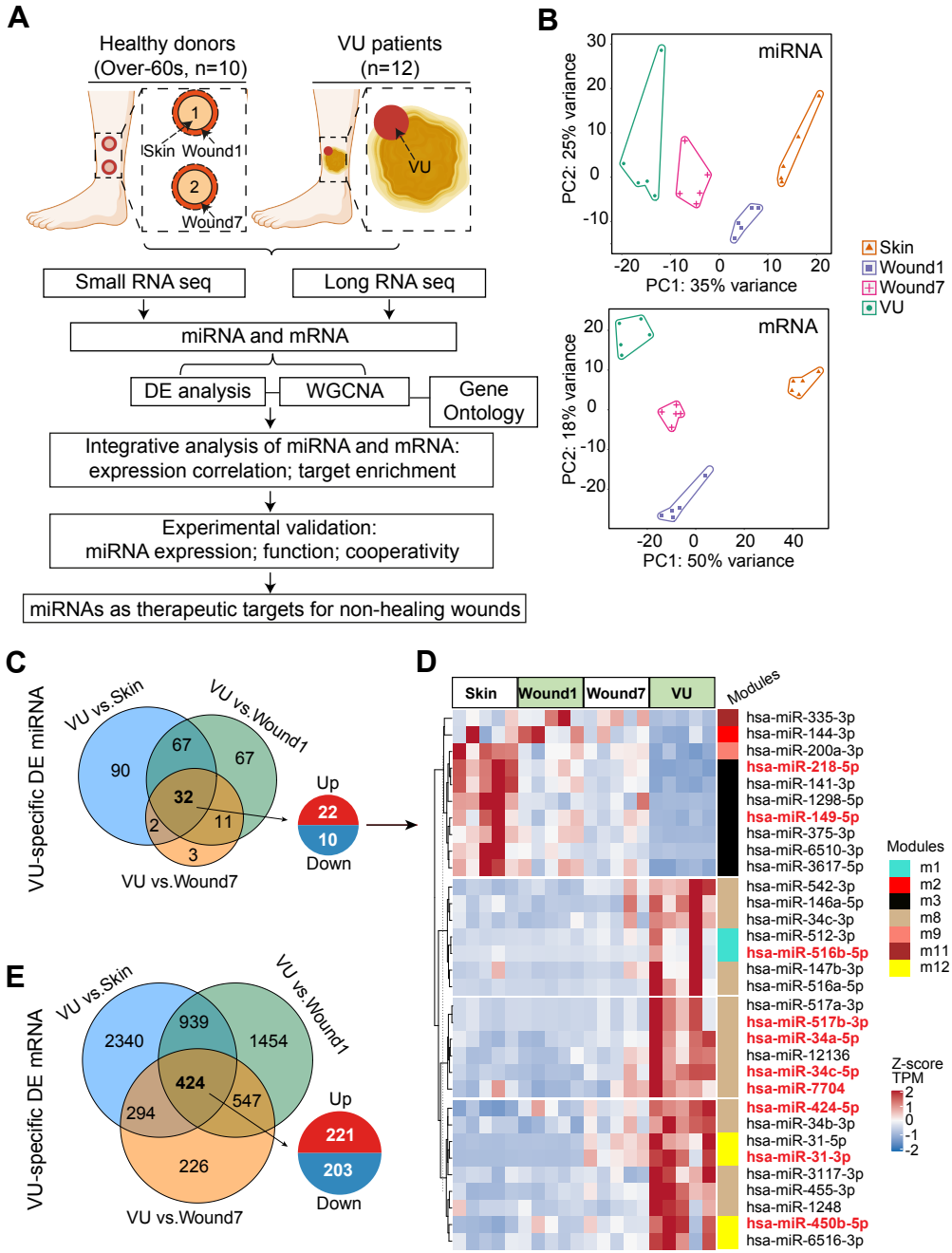

Figure 1. Paired profiling of miRNA and mRNA expression in human wounds.

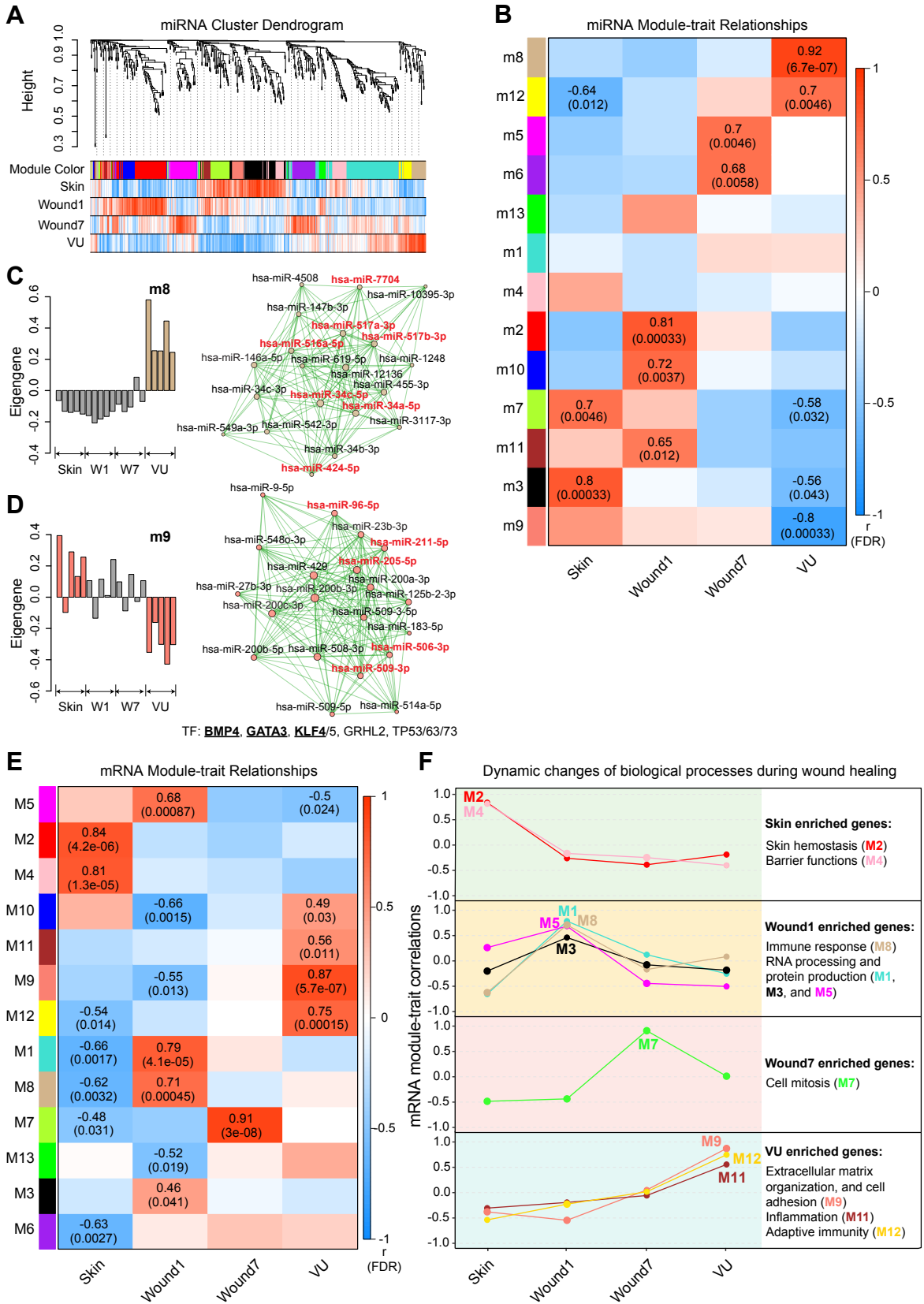

Figure 2. Weighted gene co-expression network analysis (WGCNA) of miRNAs and mRNAs in wound healing.

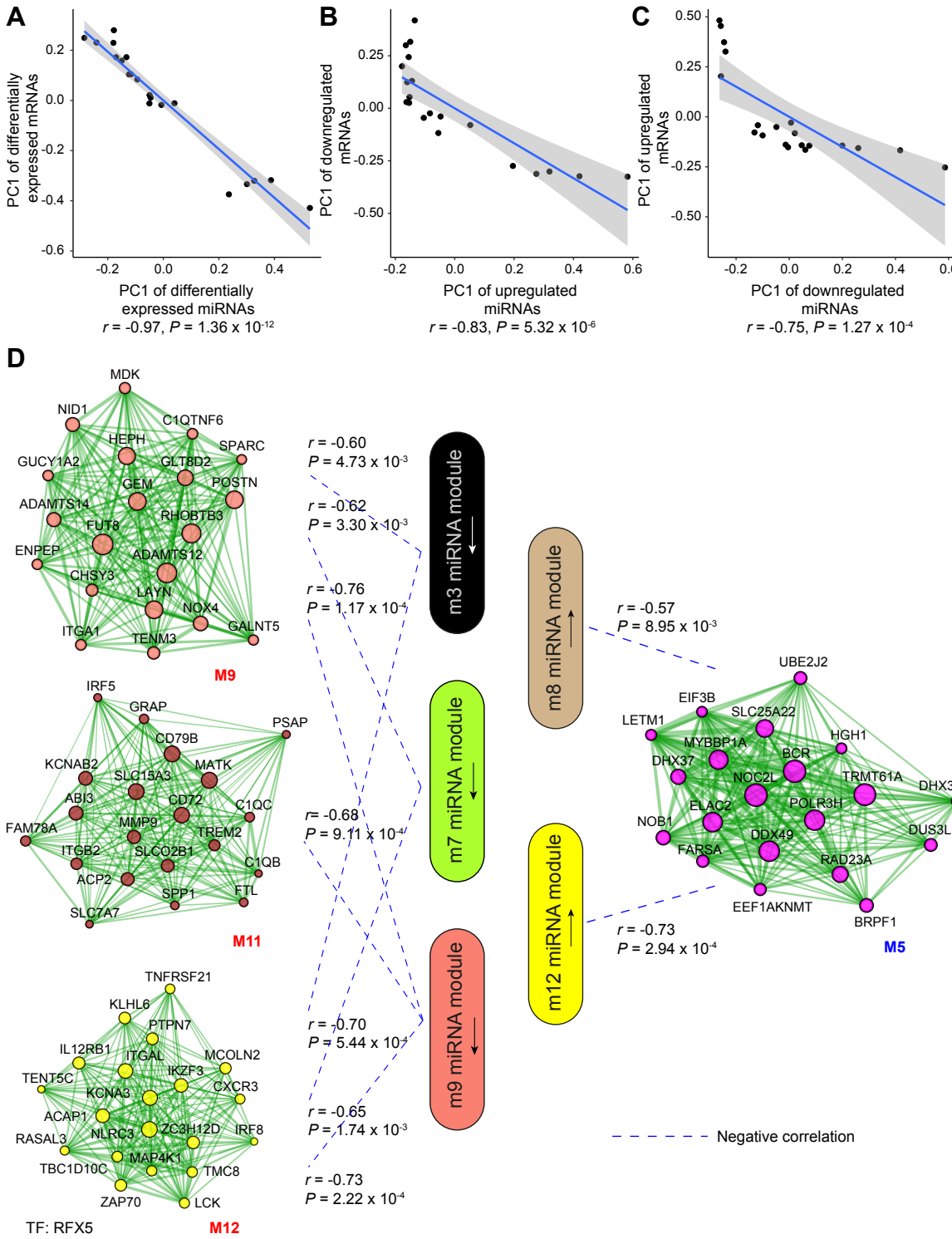

Figure 3. Correlation analysis between miRNA and mRNA expression changes in VU.

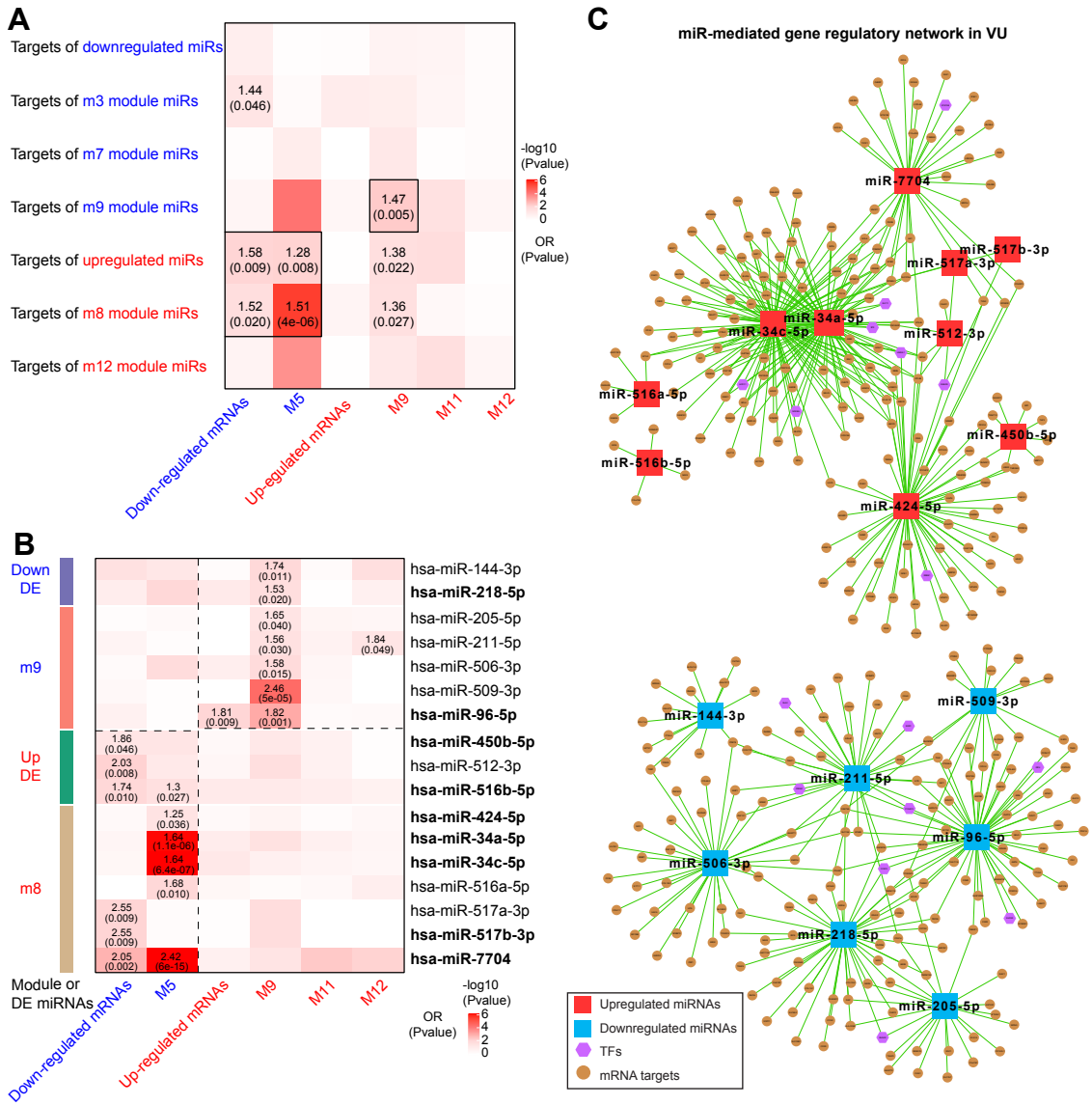

Figure 4. Integrative analysis of miRNA and mRNA expression changes in VU.

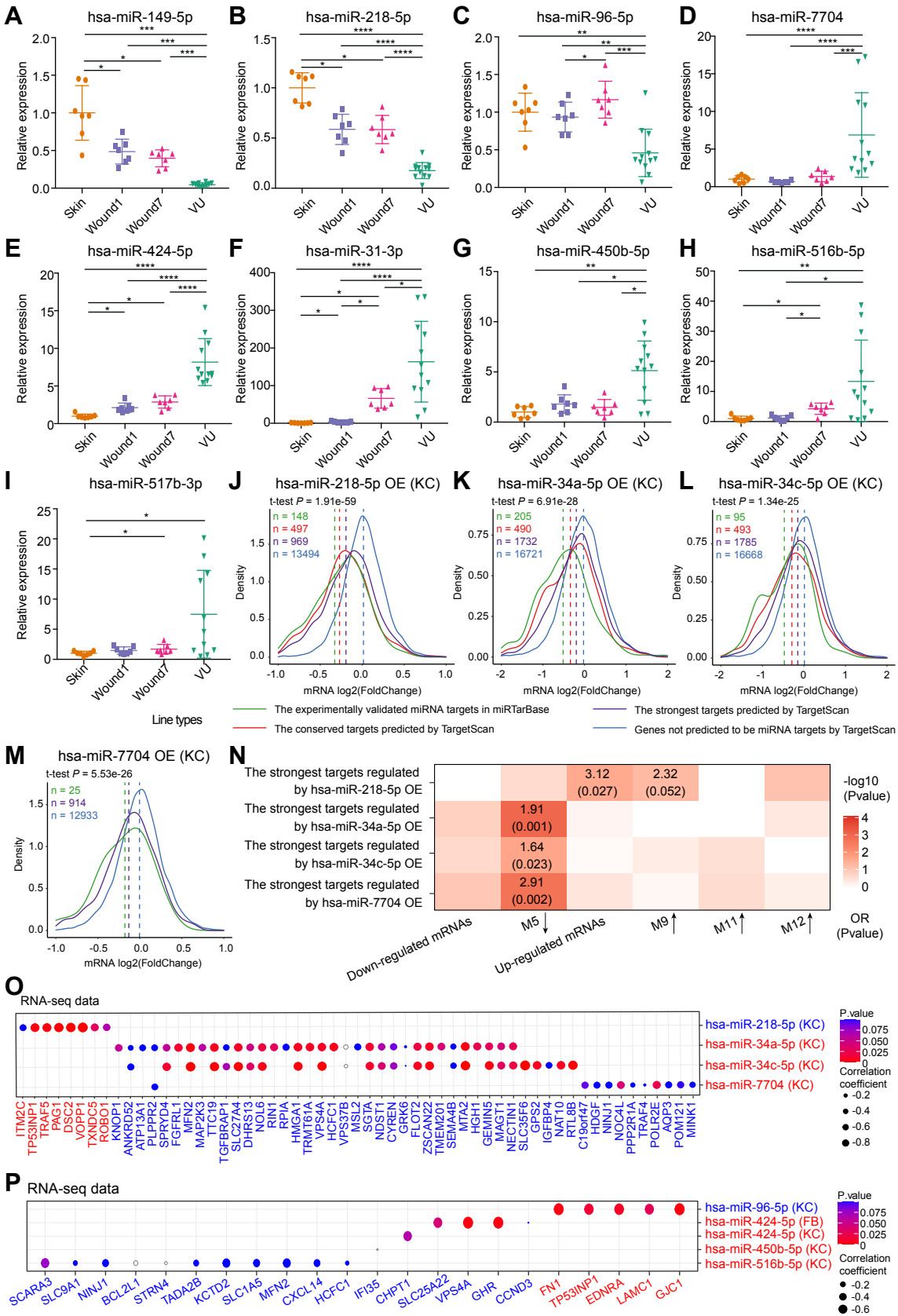

Figure 5. Experimental validation of miRNAs' expression and targets in human skin wounds.

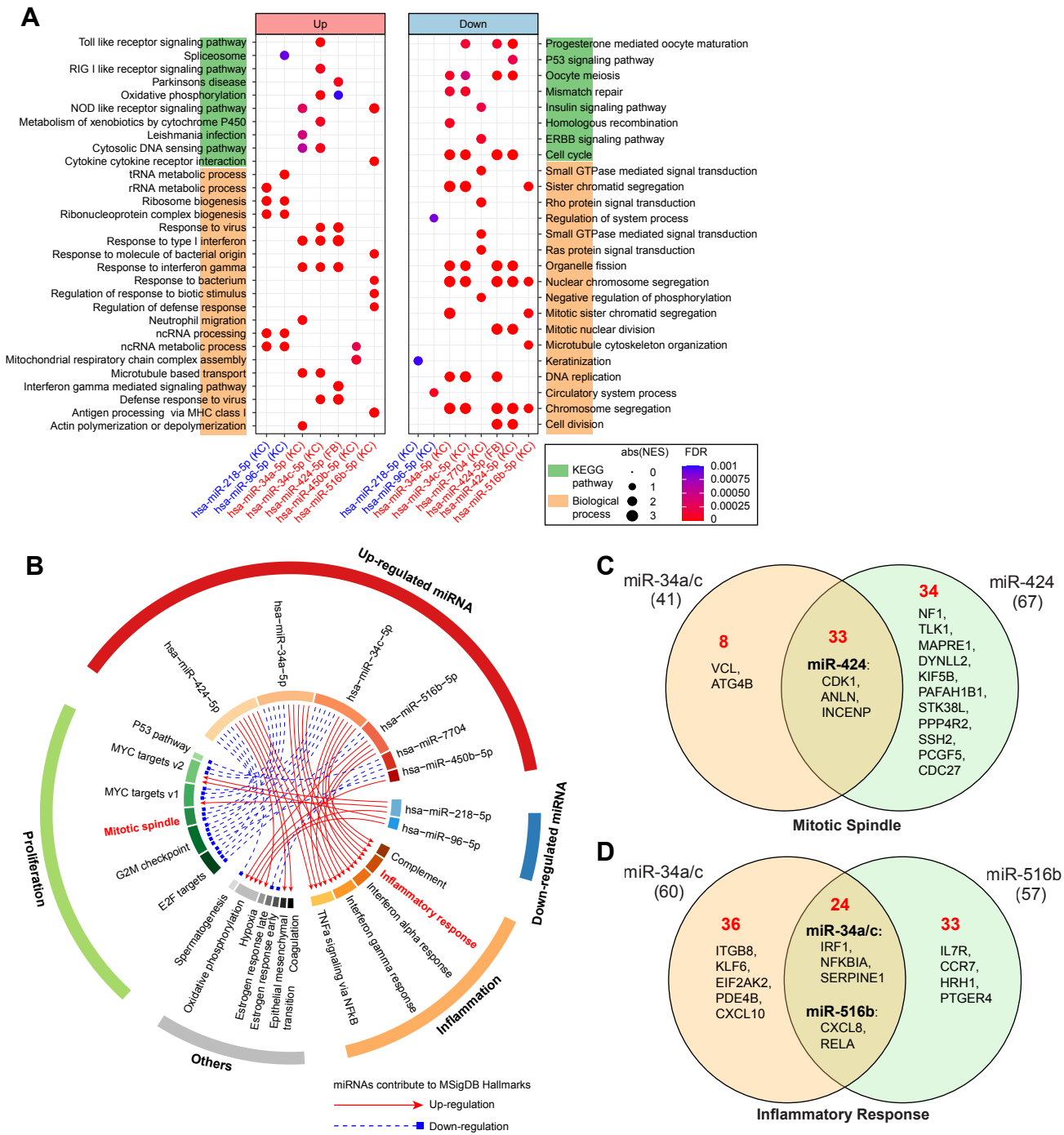

Figure 6. Cooperativity of VU pathology-relevant miRNAs.

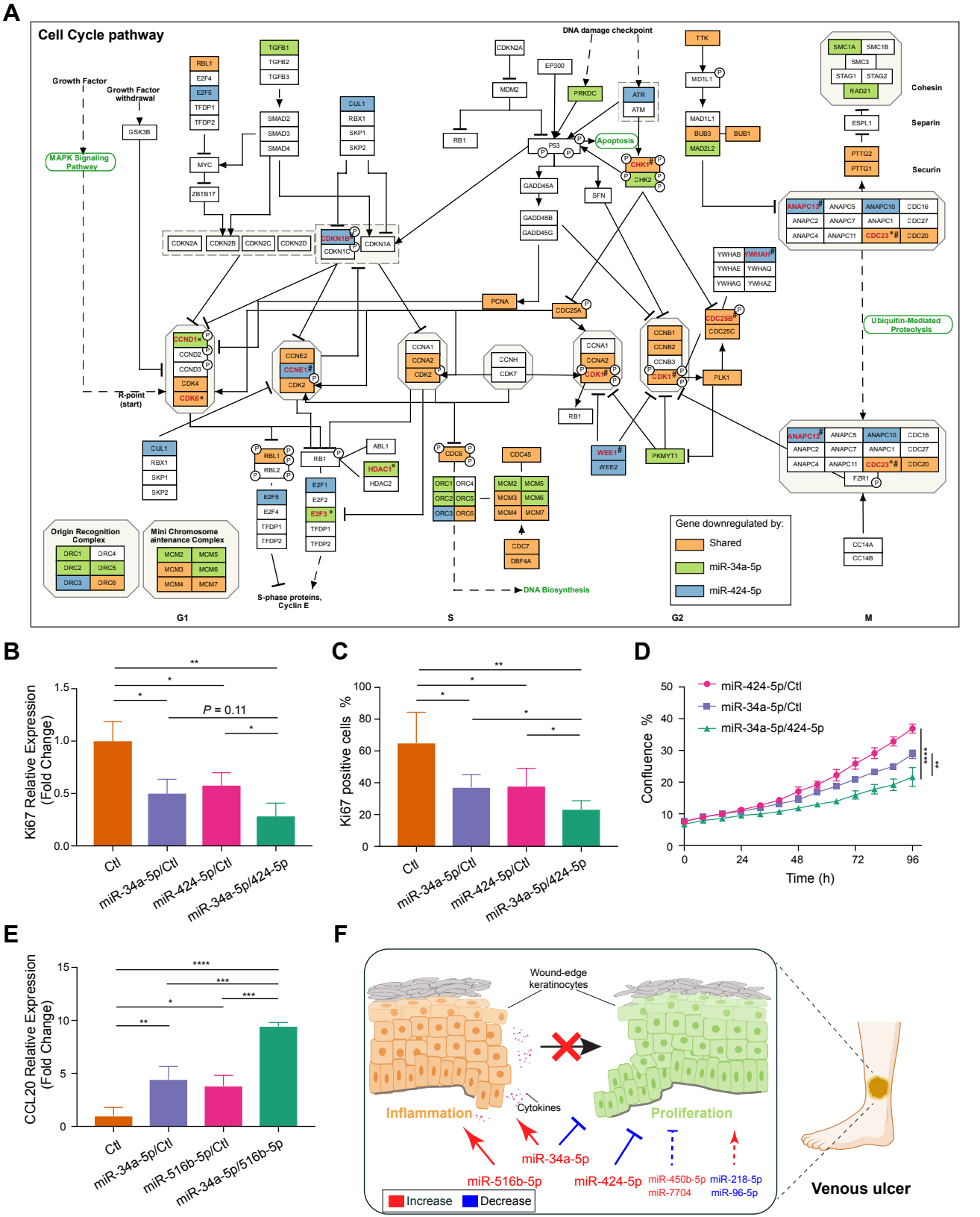

Figure 7. Cooperation of miR-34a, miR-424, and miR-516 in regulating keratinocyte proliferation and inflammatory response.